Proc. Natl. Acad. Sci. USA
Vol. 86, pp. 1254–1258, February 1989
Cell Biology

Fourier analysis of cell motility: Correlation of motility with metastatic potential

(prostate/cancer/Dunning R3327/cell shape)

ALAN W. PARTIN*†, JOSEPH S. SCHOENIGER‡, JAMES L. MOHLER*§, AND DONALD S. COFFEY*†¶

¶The Oncology Center and the Departments of *Urology, †Pharmacology, and ‡Biological Chemistry, The Johns Hopkins University School of Medicine, Baltimore, MD 21205

Communicated by Sheldon Penman, October 17, 1988

ABSTRACT **We report the development of a computerized, mathematical system for quantitating the various types of cell motility. This Fourier analysis method simultaneously quantifies for individual cells (*i*) temporal changes in cell shape represented by cell ruffling, undulation, and pseudopodal extension, (*ii*) cell translation, and (*iii*) average cell size and shape. This spatial–temporal Fourier analysis was tested on a series of well-characterized animal tumor cell lines of rat prostatic cancer to study in a quantitative manner the correlation of cell motility with increasing *in vivo* metastatic potential. Fourier motility coefficients measuring pseudopodal extension correlated best with metastatic potential in the cell lines studied. This study demonstrated that Fourier analysis provides quantitative measurement of cell motility that may be applied to the study of biological processes. This analysis should aid in the study of the motility of individual cells in various areas of cellular and tumor biology.**

Cell motility is often used synonymously with cell translation, yet translation represents only one of the many types of cell movement. Cell motility may involve membrane ruffling and undulation, pseudopodal extensions (i.e., blebs, filopodia, or leading lamellae), or various types of translation including random or persistent cell walks. These types of motility may be expressed after several types of biological stimulation. For example, oncogenes (1–4), hormones (5), and various growth factors (6–7) have been demonstrated to induce membrane ruffling in cultured cells. It is becoming apparent that quantitative information describing these types of cell movement is needed to study and understand better the processes of cell motility.

Several techniques and various mathematical approaches have been used to quantify cell translation [e.g., the Boyden chamber (8), phagokinetic tracks (9), the under-agarose method (10), the Markov chain model (11), cell diffusional coefficients (12), and analysis of cell centroid (13); for reviews, see refs. 14 and 15]. These methods analyze motility by studying static representations of cell translation but fail to describe accurately the dynamic nature of the processes involved in cell movement. Time-lapse video recordings of cell movements have provided visual information on the various types of cell motility and have allowed the development of subjective classification schemes (16). Unfortunately, the overwhelming quantity of data provided by time-lapse video techniques has made extraction of useful quantitative information difficult.

The types of motility exhibited by individual cells mimic a wave-form motion that may be analyzed by several mathematical techniques (14, 15). The complex shape of a cell contour can be decomposed into spatial harmonics that are the sinusoidal frequencies that produce that shape. Fourier analysis of cell contours utilizes a Fourier transform to provide a mathematical representation of a cell shape by reduction into its component sine and cosine Fourier coefficients. We report the development of a mathematical, computerized image analysis method utilizing a spatial–temporal Fourier analysis that is capable of analyzing time-lapse data and that provides accurate, quantitative information on the various types of cell motility. We have applied this method to the study of tumor cell metastasis in the Dunning R3327 rat model of prostatic cancer.

RESULTS AND DISCUSSION

Cell Culture, Microscopy, and Image Analysis. Fig. 1 is a flow diagram of the procedure. Cells from each of the low-metastatic (G, AT1, and AT2) and high-metastatic [AT3, MAT-Lu or (ML), and MAT-LyLu or (MLL)] sublines of the Dunning R3327 rat prostatic adenocarcinoma were inoculated at low density ($<10^5$ cells per plate) on plastic tissue culture flasks and equilibrated in 5% CO_2/95% air at 37°C in RPMI 1640 medium with 2 mM L-glutamine, 10% (vol/vol) fetal calf serum, 250 nM dexamethasone, penicillin G (100 units/ml), and streptomycin (100 units/ml) (17). Twelve to 24 hr after passage, flasks were sealed and transferred to a 37°C heated microscope stage. All cell lines were treated in a similar fashion.

Single cells were viewed with a high-resolution black-and-white video camera (Dage MTI, Michigan City, IN, series 66) at ×400 magnification with an inverted Zeiss (IM35) microscope (Hoffman optics) and digitized at 60-sec intervals for 64 min with a raster graphics adapter (AT&T Targa-M8) and commercially available software (ImagePro, Media Cybernetics, Silver Spring, MD). Cell contours were manually traced from the digital images with a digitizer tablet (SummaSketch MM-1201, Fairfield, CT) and their x–y coordinates were stored. The x–y coordinates for each of the 64 individual contours were interpolated to 128 equidistantly spaced points.

Fourier Analysis of Cell Motility. The coordinates were subjected to a complex fast Fourier transform to determine the spatial Fourier coefficients describing the cell shape. The spatial Fourier coefficients for each of the 64 cell contours were combined and a second temporal complex fast Fourier transform was calculated that measures the temporal fluctuations in the amplitude of the spatial harmonics (Fig. 1). This is graphically depicted in a two-dimensional plot representing the spatial–temporal Fourier analysis of the motility of a single cell. A two-dimensional object, such as a cell contour, can be represented as a one-dimensional vector of complex numbers with the x coordinate as the real component and the y coordinate as the imaginary component. The motility

The publication costs of this article were defrayed in part by page charge payment. This article must therefore be hereby marked "*advertisement*" in accordance with 18 U.S.C. §1734 solely to indicate this fact.

Abbreviations: *S*, spatial harmonic; *T*, temporal frequency.

§Present address: Division of Urology, University of North Carolina, Chapel Hill, NC 27514.

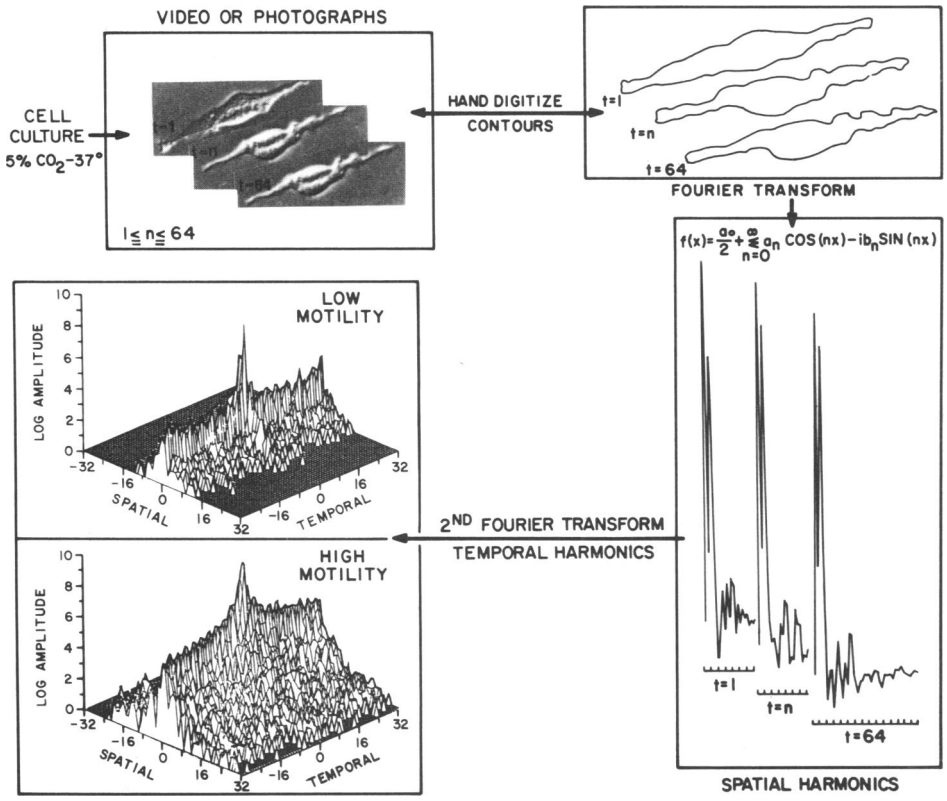

FIG. 1. Fourier measurement of the motility of single cells. Cells were digitized at 60-sec intervals for 64 min. Cell contours were manually traced from the digital images with a digitizer tablet. The coordinates were then transformed with a complex fast Fourier transform to determine the spatial Fourier coefficients describing cell shape. The spatial Fourier coefficients were combined into a matrix and a second temporal fast Fourier transform measured the temporal fluctuations in the amplitude of the spatial harmonics. This is graphically depicted in a two-dimensional plot of the spatial–temporal Fourier analysis of the motility of a single cell. For graphical representation, the log of the amplitudes of the Fourier motility coefficients are shown. The results of analysis of a highly motile cell are compared to that of a low-motility cell.

coefficients in the positive and negative quadrants, while appearing similar in the log plots, are not symmetrical and provide different information concerning the various aspects of cell motility.

The magnitude (amplitude) of a Fourier coefficient represents how much a given spatial harmonic contributes to the overall shape of the cell. Changes in cell shape can be analyzed with a second fast Fourier transform that quantifies the temporal fluctuations in the amplitude of each spatial harmonic. We have defined the amplitude at each location in the matrix as an individual Fourier motility coefficient. The location of each motility coefficient on the matrix represents the temporal frequency (T) at which that spatial harmonic (S) was changing with time. The amplitude of each motility coefficient represents how much a given spatial–temporal harmonic contributes to the overall cell movement (Fig. 1). This matrix contains a quantitative description of all cell movement occurring within the time the cell was studied.

This Fourier analysis is sensitive to the size (perimeter length) of the cell being analyzed. The amplitudes of the spatial harmonics that describe two identically shaped yet different size cells would differ proportionately. To eliminate size dependency, all Fourier motility coefficients are size-normalized by dividing by the average perimeter of the contours within the time series analyzed. This system served as a prototype for a Zeiss cell motility morphometry work station.

In a cell exhibiting low amounts of motility, the shape and location of the cell contour do not change significantly over time. The Fourier analysis of such a series of contours would result in low-amplitude temporal changes in the size of the spatial harmonics (Fig. 1). Conversely, the Fourier analysis of a highly motile cell would show high-amplitude temporal changes in the size of the spatial harmonics (Fig. 1).

Computer-Generated Models of Cell Motility. A series of animated computerized cell motility models were constructed that exhibited mathematically defined spatial, as well as temporal, amplitude and frequency changes mimicking each type of cell motility. These models were then analyzed with the Fourier technique to determine the general locations within the motility coefficient matrix of each type of cell motility.

Computer-generated models of ruffling, pseudopodal extension, and undulation were made. To determine the effect of spatial amplitude on the height and location of the Fourier motility coefficients (Fig. 2), the spatial amplitude for

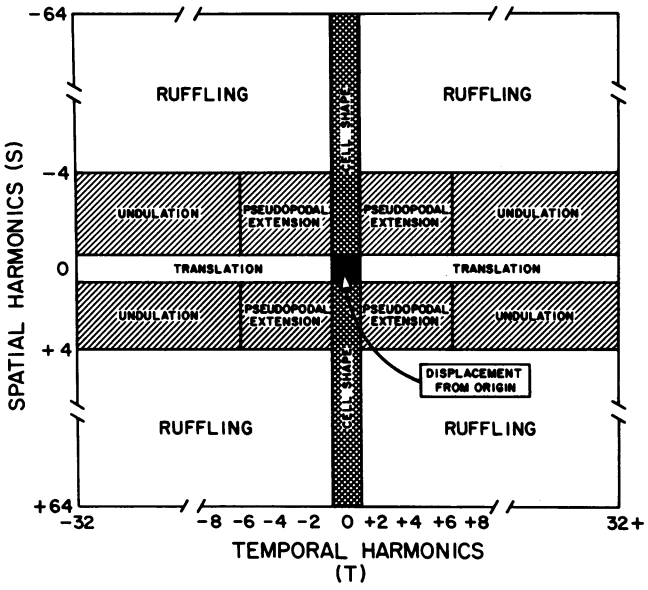

FIG. 2. Schematic diagram of the matrix of Fourier motility coefficients. The areas in the matrix that contain the Fourier motility coefficients representing undulation, ruffling, pseudopodal extension, translation, displacement from center, and cell shape are labeled in the schematic. Undulation harmonics [spatial ($S = \pm 1$–4) and temporal ($T = \pm 7$–32)], ruffling harmonics [($S = \pm 5$–64) and ($T = \pm 1$–32)], pseudopodal extension harmonics [($S = \pm 1$–4) and ($T = \pm 1$–6)], translation harmonics ($S = 0$ and all T), average displacement from origin at harmonic ($S = 0$ and $T = 0$), and cell shape (all S and $T = 0$) are shown.

pseudopodal extension, ruffling, and undulation were varied while holding spatial and temporal frequency and the amount of cell membrane and motility constant. The same experiment was repeated varying the amount of cell membrane involved in the motility event and holding the other variables constant. In brief, we observed that the amplitude and spatial–temporal location of the motility coefficients correlated directly with the values used to generate the animated models (see data below) and provided a means for identifying the general location within the matrix of Fourier motility coefficients in which each type of motility was represented.

Within any type of cell motility, events with higher temporal frequency are more likely to produce greater movement and result in increased motility. All motility coefficients within the ruffling, undulation, and pseudopodal extension areas (Fig. 2) are frequency weighted by multiplying the amplitude of the coefficient by the absolute value of the temporal frequency. Fig. 2 depicts a classification scheme for segregating the motility coefficients into discrete regions of the spatial–temporal matrix. Biologically, these movements represent a continuum whose boundaries cannot be precisely defined. The classification scheme proposed identifies the general locations within the spatial–temporal matrix representing these specific types of cell motility. The sum of all motility coefficients within the matrix for an individual cell represents the overall motility for that cell.

Fourier Analysis of Translation. Models of cell translation demonstrated that cell translation information is contained exclusively within the zero spatial harmonics (Fig. 2). The amplitude of the zero spatial ($S = 0$) and zero temporal ($T = 0$) harmonic measures the average displacement of the cell from the origin. The $\tan^{-1}$ of the Fourier coefficients at the ($S = 0$), ($T = 0$) harmonic is the angle representing the average direction (bearing) of cell translation. Analysis of the inverse Fourier transform of the Fourier coefficients of all zero spatial harmonics ($S = 0$ at all T) provides quantitative information on cell translation (e.g., final displacement and total displacement). This information can be used to distinguish directionally persistent from random cell walks (12). We tested the ability of this Fourier technique to determine two manually measurable translation parameters (average displacement from origin in micrometers and average bearing in degrees). The spatial–temporal Fourier technique provided values equal to the manually measured values. The results for the manually measured average displacement from origin are compared with those determined by the Fourier method and correlated perfectly (correlation coefficient, 1.00). The results for the average bearing (data not shown) also showed equivalent values. All motility coefficients, taken before size normalization, in the ($S = 0$) harmonics were summed to yield a value depicting the overall Fourier translation of the cell.

Fourier Analysis of Average Cell Shape. Average cell shape information is contained within the zero temporal harmonics (Fig. 2). The inverse transform of the Fourier coefficients comprising the cell-shape harmonics (all values of S at $T = 0$) produces x–y coordinates that represent the average cell shape during the time series analyzed. Morphometric analysis of this average contour provides the average area, perimeter, and shape of the cell being analyzed. This information can be useful for discriminating between cell types with characteristically different shapes (18).

Model of Pseudopodal Extension. An accurate standard to measure ruffling, undulation, and pseudopodal extension does not exist for testing the results of the Fourier motility coefficients. For this reason we analyzed computer-generated models of cell motility. When cells are viewed by time-lapse videomicroscopy, pseudopodal extension is characterized by long extensions and retractions of cell membrane that occur with low frequency. Therefore, pseudopodal extension, represented in our computerized animated models by large-amplitude low-frequency changes in cell shape, produced time-dependent changes in the lower spatial ($S = \pm 1$–4) and temporal ($T = \pm 1$–6) harmonics (Fig. 2).

To determine the effects of increasing pseudopod length (spatial amplitude) on the Fourier motility coefficients within the pseudopodal area, a series of computer-generated models were created. Within these models, we varied the length of a pseudopod from 0.1 to 0.9 arbitrary units while holding constant the spatial frequency at 0.50 cycle and temporal frequency at 0.25 cycle. Fig. 3*B* demonstrates that, as the amplitude of the pseudopod increased, the Fourier pseudopodal index increased proportionally and identifies the general location within the Fourier motility coefficient matrix in which pseudopodal extension was located.

To determine the effects of increasing the amount of total cell contour involved in making the pseudopod on the Fourier motility coefficients, a series of computer-generated models were created. We varied the percent of cell contour occupied by the pseudopod from 3% to 50% of the total contour while holding constant the spatial frequency at 0.50 cycle, temporal frequency at 0.25 cycle, and spatial amplitude at 1.0 arbitrary unit. Fig. 3*A* demonstrates that, as the percent of cell contour occupied by the pseudopod increased, the Fourier pseudopodal index decreased proportionally. These data demonstrate that, as the amount (percent) of total cell contour occupied by the pseudopod increased, the values for the Fourier pseudopod index decreased proportionately demonstrating that the Fourier method for measuring pseudopodal extension is weighted toward pseudopods that are more spike-like (occupy a smaller percent of the total cell contour).

Model of Membrane Ruffling and Undulation. Undulation occurs over large portions of the cell membrane but is of lower amplitude and higher frequency than pseudopodal extension. Undulation, represented in our animated models by medium-amplitude high-temporal frequency changes in the cell membrane, produced time-dependent changes in the lower-spatial ($S = \pm 1$–4) and higher-temporal ($T = \pm 7$–32) harmonics (Fig.

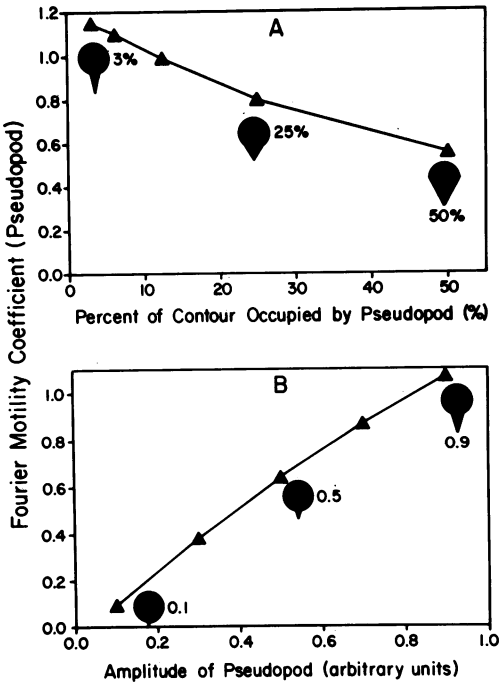

FIG. 3. Analysis of varying pseudopod length and percent of cell contour on the Fourier motility coefficients. (*A*) Correlation of the Fourier pseudopod index with increasing percent of total cell contour occupied by the pseudopod. (*B*) Correlation of the Fourier pseudopod index with increasing spatial pseudopod length (spatial amplitude).

2). Ruffling, characterized as high-frequency and lower-amplitude cell membrane changes, was modeled in a similar fashion and caused small time-dependent changes in the temporal harmonics ($S = \pm 5$–64) and ($T = \pm 1$–32) (Fig. 2).

Various computer models demonstrating membrane ruffling and undulation were generated. Within these models, the spatial amplitude of the ruffling, the temporal frequency at which the change occurred, the spatial frequency of the membrane change, and the amount of total cell contour involved in the motility were all singly analyzed in a fashion similar to that shown above for pseudopodal extension. Fig. 4*B* demonstrates that the Fourier motility ruffling index increases proportionally to the increase in amplitude (height) of the ruffles. Fig. 4*A* shows that the Fourier motility ruffling index, unlike that shown in the pseudopod experiment, increases as the percent of total cell contour increases. Models of undulation demonstrated similar results.

Study of Control (Nonmotile) Cells. To determine the error due to manual digitization inherent with this technique, the same cell image was hand-digitized 64 times, representing a cell with no motility. These contours were then analyzed with the spatial–temporal Fourier transform and formed a control blank for this technique. The motility coefficients representing cell shape change and translation with this blank had minimal noise and the values were less than one-third of the very lowest motility values calculated for a cell.

Visual Motility Grading. Cell contours (64 for each of 156 Dunning cells) were graphically displayed on the computer monitor in rapid succession (1 contour per 2 sec) to mimic the movements of the cell. Three parameters of cell motility were graded visually. The three motility parameters (ruffling, pseudopodal extension, and translation) were subjectively graded from 0 (no motility) to 5 (large amounts of observed motility). Each visual motility parameter was tested for its correlation with values obtained with the Fourier method of quantifying cell motility with linear correlation coefficients.

Comparison of Visual Grading and Fourier Analysis of Cell Motility. To determine whether this Fourier method for measuring cell movement could accurately discriminate between the visually observed types of motility when applied to live cancer cells, we selected 156 Dunning prostate cancer cells and visually graded (subjectively) each cell for the amount of ruffling, undulation, pseudopodal extension, and overall translation from 0 to 5. For comparison the visually graded cells were then analyzed with the spatial–temporal Fourier transform. The results of this visual grading of individual cell motility are shown graphically in Fig. 5. Correlation coefficients of 0.77, 0.75, and 0.71 were obtained for the correlation between the subjective visual grading and the Fourier method (Fig. 6) when determined independently for ruffling, pseudopodal extension, and translation, respectively. These correlations indicate that this Fourier method can discriminate among these types of cell motility and validates the classification scheme proposed above for the motility coefficients.

This demonstrates the specificity of the new Fourier technique to recognize the various forms of motility. What is the true standard? The eye can visualize the cell movement but the subjective visual grading is not precise. The Fourier

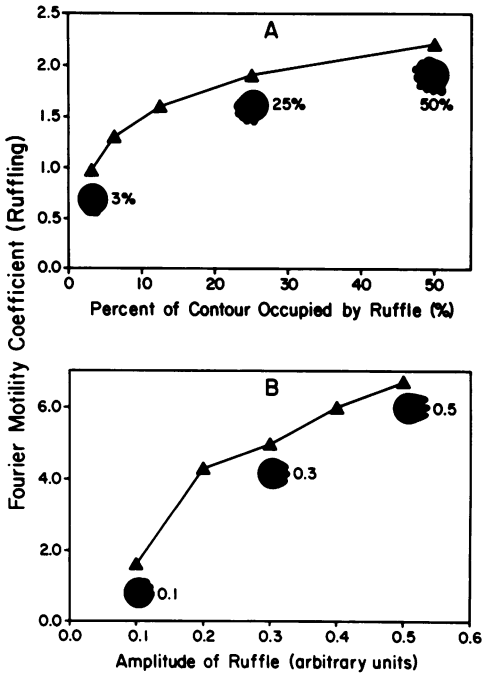

FIG. 4. Analysis of various ruffling parameters on the Fourier motility coefficients measuring ruffling. (*A*) Correlation of the Fourier ruffling index with increasing percent of total cell contour occupied by ruffle. (*B*) Correlation of the Fourier ruffling index with increasing spatial amplitude of cell contour ruffle.

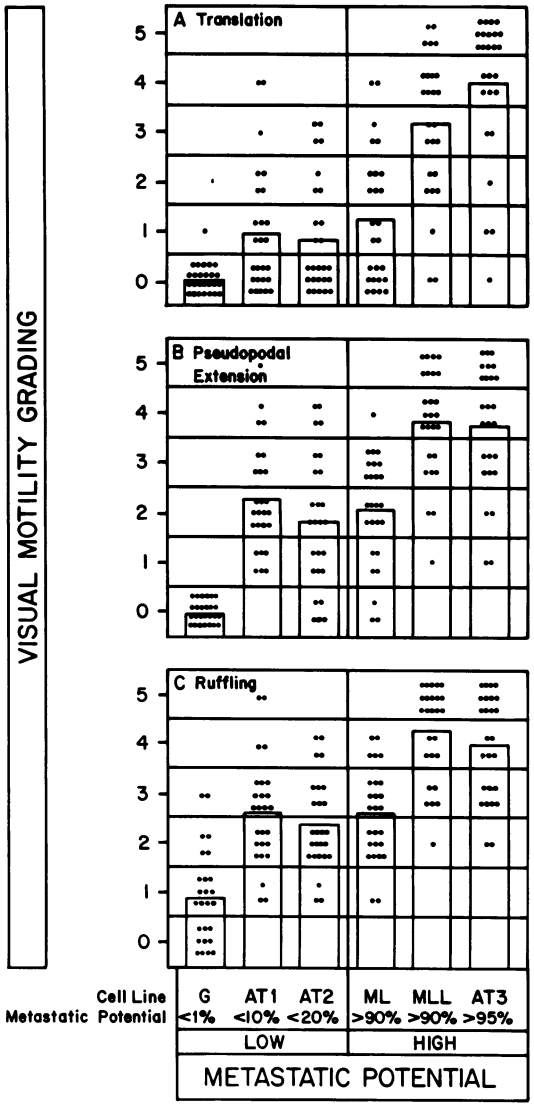

FIG. 5. Visual grading of cell motility for 26 cells from each of the six Dunning cell lines. Overall translation (*A*), pseudopodal extension (*B*), and cell membrane ruffling (*C*) were visually graded from 0 to 5 individually for 26 cells from each of the six Dunning cell lines. Dots represent the grading of an individual cell. Metastatic potential is expressed as the percent of animals developing distant metastases at 42 days after s.c. injection of 10^5 cells into the animal's flank.

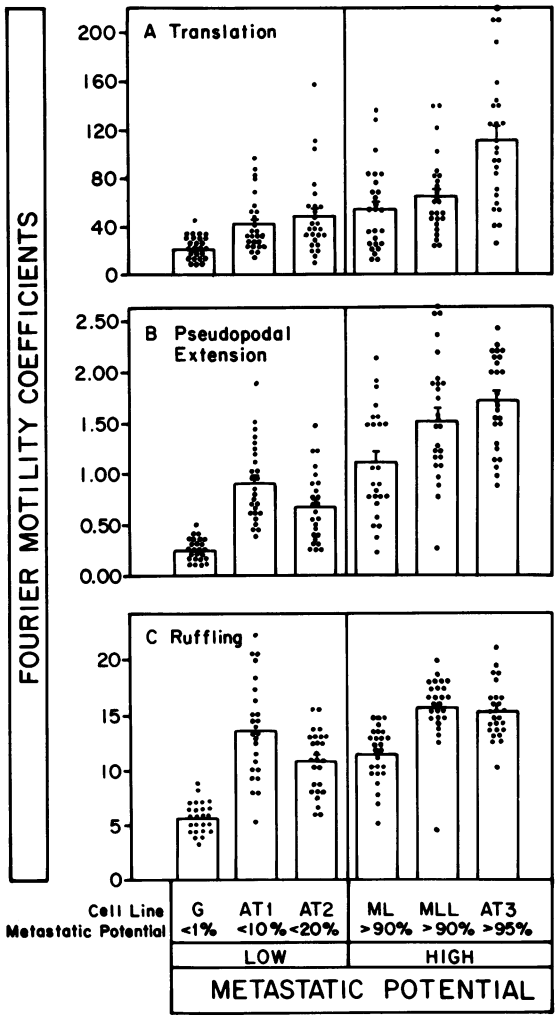

FIG. 6. Comparison of Fourier motility coefficients for six Dunning tumor cell lines with various metastatic potential. Twenty-six cells from each of six Dunning cell lines were analyzed with the spatial–temporal Fourier method described in Figs. 1 and 2. Fourier motility coefficients were determined for translation (*A*), pseudopodal extension (*B*), and ruffling (*C*). Metastatic potential is arbitrarily defined as low metastatic when <20% of rats develop distant metastases and high metastatic when >90% develop distant metastases. Bars represent the mean ± SEM for 26 cells from each cell line.

method is quantitatively precise but the resolution is not equivalent to the eye. The true standard would be ultimately a high-resolution image analysis and optical system analyzed by mathematical methods such as this Fourier technique.

Correlation of Fourier Motility with Metastatic Potential. Tumor metastasis is a complex and poorly understood multifactorial process involving many cellular activities (19–25). Cell motility may have an essential role in metastasis (16, 20, 22, 23, 25). Guirguis *et al.* (26) reported that an autocrine motility factor stimulates the formation of pseudopodal protrusions from cancer cells. Previously, we combined (16) time-lapse videomicroscopy and a subjective visual grading system of cell motility to correlate membrane ruffling, pseudopodal extension, and cell translation with metastatic potential in an animal tumor model of prostatic cancer (17). The Dunning R3327 rat prostatic adenocarcinoma tumor model provided us with six well-characterized, clonal cell lines that were all derived from the same spontaneous rat prostate tumor (27) and have a broad range of metastatic potentials. Twenty-six cells from each of the six Dunning tumor cell lines were analyzed with our spatial–temporal Fourier method of quantifying cell motility to determine whether various types of cell motility correlated with metastatic potential.

Plots of the spatial–temporal Fourier coefficients for membrane ruffling, pseudopodal extension, and translation for cells from the Dunning lines are shown in Fig. 6. The motility coefficients for translation and pseudopodal extension were higher for cells from tumor sublines with higher metastatic potential. It is not known whether the variability of motility coefficients within each cell line may be due to tumor cell heterogeneity (28). Analysis of the correlation between the degree of metastatic potential of the tumor line and each of the various Fourier motility coefficients yielded correlation coefficients of 0.63 for pseudopodal extension ($P < 0.001$), 0.50 for translation ($P < 0.001$), and 0.50 for ruffling ($P < 0.001$).

We thank Dr. Patrick C. Walsh for his support during this project. We thank James Gurganus, Robert Pitcock, Susan Dalrymple, and Alexander Walsh for the expert collection and analysis of cell data and Drs. Steven Piantadosi, John T. Isaacs, William Guier, Nachum Gershon, Mr. Robert Jernigan, and Mr. William Geckle for their expert advice. We also thank Drs. Bert V. Vogelstein, Thomas S. K. Chang, and Evelyn R. Barrack for their critical review of this manuscript. This work was supported by Grant CA 15416 from the National Cancer Institute. A.W.P. and J.S.S. are M.D., Ph.D. candidates in the Medical Scientist Training Program and are supported by Training Grant 5T32 GM07309.

1. Porter, K. R., Torado, G. J. & Fonte, V. G. (1973) *J. Cell Biol.* **59,** 633–642.
2. Ambros, V. R., Chen, L. B. & Buchanan, J. M. (1975) *J. Cell Biol.* **72,** 3144–3148.
3. Bar-Sagi, D. & Feramisco, J. R. (1986) *Science* **233,** 1061–1068.
4. Myrdal, S. E. & Auersperg, N. (1985) *Exp. Cell Res.* **159,** 441–450.
5. Goshima, K., Masuda, A. & Owaribe, K. (1984) *J. Cell Biol.* **98,** 801–809.
6. Heine, U. I., Keski-Oja, J. & Wetzel, B. (1981) *J. Ultrastruct. Res.* **77,** 335–343.
7. Myrdal, S. E., Twardzik, D. R. & Auersperg, N. (1986) *J. Cell Biol.* **102,** 1230–1234.
8. Boyden, S. (1962) *J. Exp. Med.* **115,** 453–466.
9. Albrecht-Buehler, G. (1977) *Cell* **11,** 395–404.
10. Nelson, R., Quie, P. Q. & Simmons, R. L. (1975) *J. Immunol.* **115,** 1650–1656.
11. Boyarsky, A. (1975) *J. Math. Biol.* **2,** 1–15.
12. Gail, M. H. & Boone, C. W. (1970) *Biophys. J.* **10,** 980–993.
13. Dunn, G. A. & Brown, C. W. (1986) *J. Cell Sci.* **83,** 313–340.
14. Nobel, P. B. & Levine, M. D. (1986) *Computer-Assisted Analysis of Cell Locomotion and Chemotaxis* (CRC, Boca Raton, FL).
15. Dunn, G. A. & Brown, C. W. (1987) *J. Cell Sci. Suppl.* **8,** 81–102.
16. Mohler, J. L., Partin, A. W. & Coffey, D. S. (1987) *J. Urol.* **137,** 544–548.
17. Isaacs, J. T., Isaacs, W. B., Feitz, W. F. J. & Scheres, J. (1986) *Prostate* **9,** 261–281.
18. Heckman, C. A. (1985) *Adv. Cell Cult.* **4,** 85–156.
19. Fidler, I. J. (1987) *J. Cell Biochem. Suppl.* **11,** 92.
20. Mareel, M. M. (1980) *Int. Rev. Exp. Pathol.* **22,** 65–129.
21. Strauli, P. & Haemmerli, G. (1984) *Cancer Metastasis Rev.* **3,** 127–141.
22. Liotta, L. A. (1985) in *Important Advances in Oncology*, eds. DeVita, V. T., Hellman, S. & Rosenberg, S. A. (Lippincott, Philadelphia), p. 28.
23. Haemmerli, G. (1985) *Motility of Vertebrate Cells in Culture and in the Organism: Experimental Biology in Medicine.* ed. Wolsky, A. (Karger, New York), pp. 89–117.
24. Gey, G. O. (1954) *Harvey Lect. Series L,* 154–229.
25. Wood, S., Jr. (1965) *J. SMPTE* **74,** 737–740.
26. Guirguis, R., Margulies, I., Tarabolette, G., Schiffman, E. & Liotta, L. (1987) *Nature (London)* **329,** 261.
27. Dunning, W. F. (1961) *Natl. Cancer Inst. Monogr.* **12.**
28. Owens, A. H., Coffey, D. S. & Baylin, S. B., eds. (1982) *Tumor Cell Heterogeneity: Origins and Implications* (Academic, New York).